Available online at www.sciencedirect.com
ScienceDirect
Journal of Catalysis 245 (2007) 436–445
JOURNAL OF CATALYSIS
www.elsevier.com/locate/jcat

A density functional theory study of HCN hydrogenation to methylamine on Ni(111)

Carolina Oliva [a,*], Co van den Berg [b], J.W. (Hans) Niemantsverdriet [c], Daniel Curulla-Ferré [c]

[a] *Research and Technology Chemicals, Akzo Nobel Chemicals, Velperweg 76, 6824 BM Arnhem, The Netherlands*
[b] *Research and Technology Chemicals, Akzo Nobel Surfactants, Zutphenseweg 10, 7418 AJ Deventer, The Netherlands*
[c] *Technical University of Eindhoven, Den Dolech 2, 5600 MB Eindhoven, The Netherlands*

Received 23 September 2006; revised 31 October 2006; accepted 1 November 2006

Available online 8 December 2006

Abstract

The hydrogenation of hydrogen cyanide to methylamine on Ni(111) has been studied as a model reaction for the hydrogenation of nitriles to primary amines, using density functional theory. Hydrogen cyanide adsorbs strongly on Ni(111) with an adsorption energy of −1.50 eV with the CN bond parallel to the surface. The product of the hydrogenation reaction, methylamine, is relatively weakly adsorbed on the surface compared with the hydrogen cyanide, with an adsorption energy of −0.56 eV, very similar to the adsorption energy of ammonia, −0.41 eV. The hydrogenation reaction goes through an imine intermediate (H_2CNH) independently of whether hydrogen reacts with the carbon atom or nitrogen atom of the hydrogen cyanide molecule in the first hydrogenation step. From the imine intermediate, the hydrogenation reaction is likely to proceed via a H_3CNH species to methylamine (H_3CNH_2). On the other hand, if we explore the backward reaction, methylamine decomposition on Ni(111), our calculations show that C–H bond cleavage is slightly favored over N–H bond-breaking, leading to the formation of H_2CNH_2.

Keywords: Hydrogenation; Nitriles; Nickel; DFT; Hydrogen cyanide; Methylamine

1. Introduction

Industrial production of important amines is carried out via nitrile hydrogenation in the liquid phase at elevated hydrogen pressure. Depending on the desired product, different metal catalysts are recommended: Co, Ni, and Ru for primary amine production; Cu and Rh when secondary amines are the desired product; and Pt and Pd for tertiary amine formation. The selectivity of these reactions is especially important in primary amine production, because the byproducts thus obtained cannot be utilized economically and because the separation of primary and secondary amines is difficult due to similar boiling points. The hydrogenation of fatty nitriles and adiponitrile are important reactions of this kind. The reaction mechanism responsible for the production of primary amines implies an imine intermediate that can condensate with the final primary amine to give secondary amines as byproducts. Tertiary amines can also be obtained through an enamine intermediate. Several promoters have been described for the metal catalysts mentioned above. Mn, Ag, Zr, and Pb enhance the selectivity of Co toward primary amine production, and Pd has a similar effect on Ni. It has also been observed that the support used in combination with those metals is not crucial for the selectivity [1,2]. The influence of the structure of the nitriles on the kinetics and selectivity has also been investigated [3,4]. In addition to the hydrogenation of nitriles in the liquid phase, the hydrogenation of acetonitrile in the gas phase has been studied as well [5,6]. The theoretical literature on the hydrogenation of nitriles is rather scarce; we have found only one reference dealing with the hydrogenation of acetonitrile on Ni(100) using extended Hückel calculations [7]. To the best of our knowledge, there are no theoretical papers studying the hydrogenation of nitriles to amines.

The adsorption of HCN on single crystals has been studied using several experimental techniques, including near-edge X-ray fine structure (NEXAFS) [8], high-resolution electron energy loss spectroscopy (HREELS) [8,9], reflection–absorp-

* Corresponding author.
E-mail address: carolina.oliva.garcia@gmail.com (C. Oliva).

0021-9517/$ – see front matter
doi:10.1016/j.jcat.2006.11.001

tion infrared spectroscopy (RAIRS) [10,11], secondary-ion mass spectroscopy (SIMS) [12,13], X-ray photoelectron spectroscopy (XPS) [9], Auger electronic spectroscopy (AES) [14], temperature-programmed reaction spectroscopy (TPRS), and temperature-programmed desorption (TPD) [9,11–18]. Most of these papers focus on determining whether HCN adsorbs via the lone pair of the nitrogen atom in a perpendicular orientation or parallel to the surface. For example, it has been reported, using NEXAFS and HREELS [8], that HCN adsorbs molecularly on Pd(111) with the CN bond parallel to the surface. However, TPD experiments show two desorption features at 150 and 400 K; the low-temperature feature corresponds to the HCN adsorbed via the lone pair of the nitrogen atom in a perpendicular orientation, whereas the high temperature feature was associated with the recombination of atomic hydrogen and CN [17]. On the other hand, two desorption features have also been reported for HCN on W(100): a low-temperature feature associated with HCN adsorbed in a perpendicular orientation, and a high-temperature feature ascribed to HCN adsorbed parallel to the surface [9]. HCN adsorption has also been studied on Cu(100) [10,11] and Pt(111) [11]; experiments showed that HCN adsorbs only in a perpendicular orientation. HCN has been reported to react on Pt(111), yielding NCH_2 and CN, whereas CN bond cleavage has been reported on Ni(111) [14], Ru(0001) [15] and W(100) [9,16]. To the best of our knowledge, there are just a few theoretical papers studying the adsorption of HCN on single crystals; Yang and Whitten studied the adsorption of HCN and HNC on Ni(111) using the complete active space self-consistent field method (CASSCF) and the embedding cluster approach [19]. More recently, DFT cluster model calculations were done to study the adsorption of HCN on Cu(100) [20].

Several experimental studies have reported the adsorption and decomposition of methylamine using several techniques: TPD and TPRS studies on Ni [21–23], Pt [24,25], Pd [26] and W [27], XPS on Pd [26], RAIRS on Ni [28,29] and Fe [28], angle-resolved ultraviolet photoelectron spectroscopy (ARUPS) on Pt [24], AES on Rh [30], EELS on Ni [31], and SIMS on Pd [26]. Dehydrogenation of methylamine has been observed on Ni(111) [21]. It has been reported that the CH bond is broken before the NH bond, demonstrating that the CH bond is less stable than the NH one [21,22]. The opposite behavior has been found for other metals, such as Pd(111) [26] and Pt(111) [24]. Interestingly, the ability to form secondary and tertiary amines seems to be easier on those metals in which the NH bond is less stable than the CH bond. On the other hand, the decomposition of methylamine through C–N bond scission instead of dehydrogenation takes place on Ni(100) and Cr(111) [23,28,31]. The ability to break the CN bond could be related to the different adsorption sites for methylamine on these surfaces [29,31]. The C–N bond cleavage of methylamine on several metal surfaces has been studied theoretically [32].

In this work, we use density functional theory (DFT) and the slab model approximation to study the hydrogenation of nitriles to primary amines on nickel catalysts. The (111) surface of nickel has been chosen to model the nickel catalyst and hydrogen cyanide as a model molecule containing the nitrile group; HCN has been chosen because it is the smallest molecule that contains the nitrile group, which allows us to work with smaller unit cells, translating into less computational needs. We report here the adsorption modes of HCN, CH_3NH_2, and all of the intermediate species involved in the hydrogenation reaction of HCN on Ni(111) using DFT. The adsorption energies, energy barriers, and adsorption geometries of all the species studied are discussed. The minimum energy reaction pathways for the hydrogenation of hydrogen cyanide to methylamine are also described here.

2. Computational details

We have used the Vienna ab initio simulation package (VASP) [33,34], which performs an iterative solution of the Kohn–Sham equations in a plane-wave basis set. Plane waves with a kinetic energy $\leqslant$300 eV were included in the calculation. The exchange-correlation energy was calculated within the generalized gradient approximation (GGA) using the form of the functional proposed by Perdew and Wang [35,36], usually referred to as Perdew–Wang 91 (PW91). The electron–ion interactions for C, N, H, and Ni are described by the projector-augmented wave (PAW) method developed by Blöchl [37]. This is essentially an all-electron frozen-core method combining the accuracy of all-electron methods and the computational simplicity of the pseudopotential approach, especially in the implementation of Kresse and Joubert [38]. A first-order Methfessel–Paxton smearing function with a width of about 0.1 eV was used to account for fractional occupancies [39]. Spin-polarized calculations were done to account for the magnetic properties of nickel. The relative positions of the metal atoms were fixed initially as those in the bulk, with an optimized lattice parameter of 3.5217 Å for nickel. The optimized lattice parameter was calculated using the smallest unit cell that can be used to model the bulk of Ni, and its reciprocal space was sampled with a $(15 \times 15 \times 15)$ k-point grid generated automatically using the Monkhorst–Pack method [40]. The calculated magnetic moment of fcc Ni at the equilibrium lattice constant is $0.626\mu_B$, in good agreement with the experimental value of $0.606\mu_B$ reported by Kittel [41].

The Ni(111) surface was modeled with a four-layer slab model with four nickel atoms per metal layer representing a $p(2 \times 2)$ surface unit cell and a vacuum region of $\sim$10 Å. The reciprocal space of the $p(2 \times 2)$ unit cell was sampled with a $(5 \times 5 \times 1)$ k-points grid generated automatically using the Monkhorst–Pack method. Partial geometry optimizations were performed, including relaxation of the first metal layer, using the RMM-DIIS algorithm [42]. In this method, the forces on the atoms and the stress tensor were used to determine the search directions for finding the equilibrium positions. Geometry optimizations were stopped when the difference in the total energy in two consecutive steps was $<$0.001 eV. The location of the transition states was done in two steps: (1) using the climbing-image nudget elastic band method (CI-NEB) [43], with five images generated by linear interpolation between reactants and products, to find likely transition state structures, and

(2) refining the structure of the transition state by performing a geometry optimization calculation using as starting geometry the highest-energy image and a convergence criterion based on the forces acting on the atoms. The transition state structure was converged when the forces acting on the atoms were all <0.04 eV/Å for the various degrees of freedom set in the calculation.

The molecules in the gas phase (needed to obtain adsorption energies) have been calculated using a $10 \times 10 \times 10$ Å^3 cubic unit cell. Spin-polarized calculations were performed when needed. A Gaussian smearing function with a width of 0.01 eV was used to account for fractional occupancies.

3. Results and discussion

3.1. Hydrogen cyanide (HC≡N)

HCN is likely to adsorb either perpendicular to the metal surface through the lone pair of the nitrogen atom or flat with the CN bond parallel or tilted with respect to the surface. In the latter configuration, both the carbon and nitrogen atoms interact with the surface metal atoms (Fig. 1). We calculated the adsorption of the HCN molecule at different adsorption sites considering both orientations. Our results for HCN show that the parallel adsorption modes are energetically favored compared with the perpendicular modes (Table 1). The most stable adsorption state corresponds to HCN adsorbed on a hollow site parallel to the Ni(111) surface that we refer to as f-η^3(N)-h-η^3(C), where f represents fcc and h represents hcp. η^3(N) indicates that the nitrogen atom interacts with three surface atoms. In this configuration, both nitrogen and carbon atoms are located in two adjacent fcc and hcp sites, respectively. The adsorption energy of HCN in the parallel modes varies between -0.90 and -1.50 eV. In the case of the perpendicular modes, adsorption energies between -0.34 and -0.58 eV were obtained, with the t-η^1(N), or simply the top site, being the most stable.

The HCN molecule adsorbed perpendicularly via the N atom on a top site is perturbed only slightly with respect to the gas-phase structure and has a C–N distance of 1.17 Å and a C–H distance of 1.07 Å. These values are very similar to those of the calculated HCN molecule in the gas phase and also similar to those reported experimentally [44] (Table 1). The same trend was found for HCN adsorbed on a bridge site and on threefold hollow sites (hcp and fcc) perpendicular to the surface. Greater activation of the CN bond was found for HCN in parallel configurations; in these cases the CN distance can be as large as 1.34 Å, representing an elongation of the CN distance of 0.18 Å with respect to HCN in the gas phase. For the parallel configurations, the calculated HCN angle lies between 121° and 128° in all cases, which is clearly an indication of sp^2 hybridization

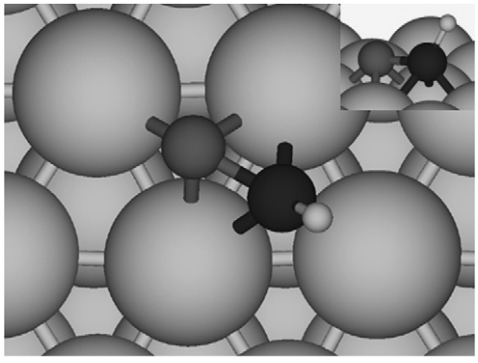

(a)

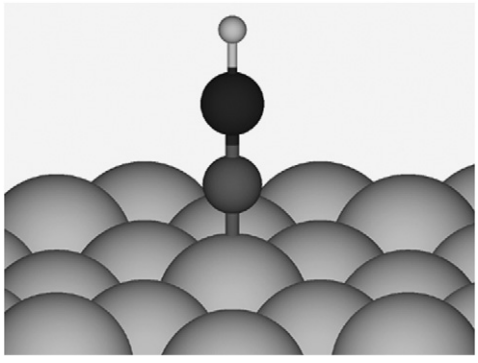

(b)

Fig. 1. Adsorption of HCN on Ni(111): (a) parallel to the surface, f-η^3(N)-h-η^3(C) and (b) perpendicular at top sites, t-η^1(N).

Table 1
HCN adsorption on Ni(111) in both perpendicular (⊥) and parallel orientations (=)

Configuration		E_{ads} [a] (eV)	d_{CN} [b] (Å)	d_{CH} (Å)	∠HCN (°)	z-N[c] (Å)	z-C[c] (Å)
⊥	t-η^1(N)	−0.58	1.17 (0.01)	1.07	180	1.96	–
	b-η^2(N)	−0.36	1.19 (0.03)	1.07	180	1.57	–
	h-η^3(N)	−0.34	1.20 (0.04)	1.07	180	1.40	–
	f-η^3(N)	−0.35	1.20 (0.04)	1.07	180	1.39	–
=	b-η^1(C,N)	−0.90	1.26 (0.09)	1.11	128	1.85	1.83
	h-η^2(C,N)	−1.25	1.31 (0.15)	1.11	125	1.53	1.55
	f-η^2(C,N)	−1.24	1.31 (0.15)	1.11	125	1.52	1.53
	f-η^3(N)-h-η^3(C)	−1.50	1.34 (0.17)	1.11	122	1.28	1.37
	h-η^3(N)-f-η^3(C)	−1.45	1.33 (0.17)	1.11	121	1.30	1.38
Gas phase	Calculated	–	1.16	1.08	180	–	–
	Exp. [44]	–	1.156	1.064	180	–	–

[a] Calculated as the energy of the reaction: $HCN_{(g)}$ + adsorption site → $HCN_{(ads)}$.

[b] Δd_{CN} between parentheses is the elongation of the CN bond with respect to the calculated hydrogen cyanide molecule.

[c] z-X is the height of X to the Ni(111) surface.

of both carbon and nitrogen atoms. In addition, the CH bond was also slightly activated for the parallel configurations.

In a previous experimental study, Hagans et al. [14] reported two energetically similar desorption states for HCN on Ni(111) with desorption peaks at 258 and 271 K. The activation energy of desorption was calculated for both peaks using the Chan–Aris–Weinberg method [45]; for the high temperature peak this energy was ∼0.87 eV with a preexponential factor of $10^{15\pm3}$ s^{-1}, and that of the low temperature peak was ∼0.78 eV with a preexponential factor of $10^{14\pm3}$ s^{-1}. According to our calculations, HCN preferentially adsorbs parallel to the surface at hollow sites with an adsorption energy of −1.50 eV. This adsorption energy is considerably greater than the activation energies of desorption reported by Hagans et al.

The discrepancy between the experimental and the theoretical results are probably due to the so-called "overbinding" effect that has been reported for CO and NO adsorption energies on transition metals [46–48]. The overbinding effect is a result of using the PW91 exchange-correlation functional. In the particular case of the CO molecule, it has been demonstrated that the origin of this effect is that the GGA-PW91 calculations do not reproduce the CO singlet–triplet excitation energy [49]. A similar explanation could hold for the NO molecule or in general, for any molecule in which the lowest unoccupied molecular orbital (LUMO) is a π orbital (just like HCN). Better agreement with the experimental adsorption energies for CO and NO on various transition metals has been reported when using the revised form of the Perdew–Burke–Enrzerhof (PBE) [50] exchange-correlation functional proposed by Zhang et al. (revPBE) [51] or Hammer et al. (RPBE) [52]. To estimate the extent of the overbinding effect in our case, we used the RPBE exchange-correlation functional to calculate the adsorption energy of HCN on Ni(111). For HCN adsorbed perpendicular to the surface on top sites, we obtained an adsorption energy of −0.27 eV using RPBE, which would correspond to a desorption temperature of ∼108 K [53]. On the other hand, for HCN adsorbed parallel to the surface in the f-η^3(N)-h-η^3(C) configuration, the calculated adsorption energy is −0.90 eV using RPBE, in good agreement with the experimental adsorption energies mentioned above. The influence of the overbinding effect on the adsorption energy for HCN on Ni(111) is then as large as that reported for CO and NO on several transition metal surfaces.

3.2. Methanimine ($H_2C{=}NH$)

For the imine intermediate (Table 2), only parallel configurations were considered in our DFT calculations. The most stable adsorption mode for this intermediate corresponds to a hollow site, either hcp (h-η^2(N)-η^1(C)) or fcc (f-η^2(N)-η^1(C)), where the N interacts with two Ni surface atoms and the C atom with just one Ni surface atom. The DFT adsorption energy for this configuration was −1.00 eV, 0.24 eV more stable than the other two likely configurations on hollow sites, h-η^1(N)-η^2(C) and f-η^1(N)-η^2(C), where we have the opposite situation, the N atom interacts with one Ni atom and the C atom with two Ni atoms (Fig. 2). In all of these adsorption configurations, the CN bond is enlarged approximately 0.1 Å with respect to the value of methanimine in the gas phase [54] and very close to

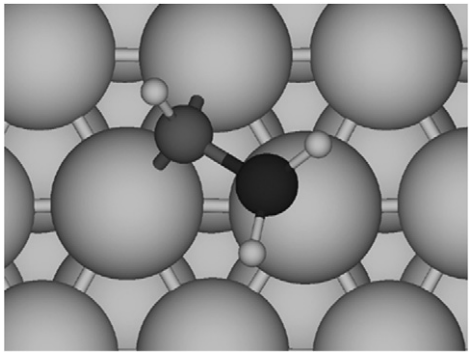

(a)

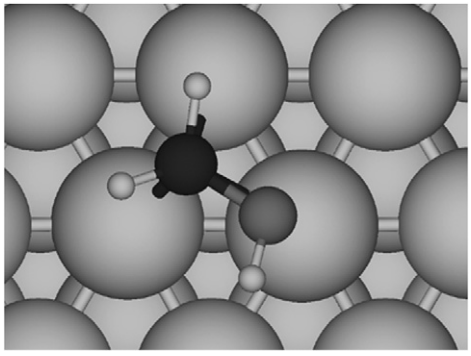

(b)

Fig. 2. Adsorption of H_2CNH on Ni(111): (a) h-η^2(N)η^1(C) and (b) h-η^1(N)η^2(C).

Table 2
H_2CNH adsorption on Ni(111)

Configuration		E_{ads}[a] (eV)	d_{CN}[b] (Å)	d_{NH} (Å)	d_{CH} (Å)	∠HCN (°)	∠HCNH (°)	z-N[c] (Å)	z-C[c] (Å)
=	b-η^1(C,N)	−0.73	1.40 (0.12)	1.03	1.11	115	144	1.97	2.06
	f-η^1(N)-η^2(C)	−0.73	1.40 (0.12)	1.04	1.13	114	144	1.98	1.74
	f-η^2(N)-η^1(C)	−1.00	1.45 (0.17)	1.03	1.11	113	90	1.52	1.89
	h-η^2(N)-η^1(C)	−1.00	1.44 (0.16)	1.03	1.11	113	90	1.52	1.89
	h-η^1(N)-η^2(C)	−0.76	1.40 (0.12)	1.03	1.14	113	146	1.92	1.72
Gas phase	Calculated	–	1.28	1.04	1.11	119	180	–	–
	Exp. [54]	–	1.273	1.023	1.081	119.7	180	–	–

[a] Calculated as the energy of the reaction: $H_2CNH_{(g)}$ + adsorption site → $H_2CNH_{(ads)}$.

[b] Δd_{CN} between parentheses is the elongation of the CN bond with respect to the calculated hydrogen cyanide molecule.

[c] z-X is the height of X to the Ni(111) surface.

the CN distance of the chemisorbed methylamine. The HCN angle and the HCNH dihedral angle for the most stable adsorption mode are 113° and 90°, respectively; thus, both carbon and nitrogen atoms are probably in a sp^x hybridization close to the ideal sp^3. One might rationalize the preference of methanimine for the h-η^2(N)-η^1(C) or f-η^2(N)-η^1(C) configurations in terms of sp^3 hybridization, because in both configurations the N and C atoms are saturated.

3.3. Methylamine (CH_3NH_2)

The adsorption of methylamine is very similar to that of ammonia; methylamine binds to the surface via the nitrogen atom lone pair on a top site. The calculated DFT adsorption energy for methylamine on Ni(111) was −0.56 eV, which translates into a desorption temperature of 224 K. This result compares well with a recent computational paper [32] and previous experimental results of Chorkendorff et al. [21] showing that methylamine desorbed between 180 and 330 K. These authors reported a saturation coverage of 3.8×10^{14} molecules/cm^2, corresponding to a surface coverage of approximately 0.20 mL. Note that our calculations were done using a $p(2 \times 2)$ unit cell, and, consequently, the surface coverage in our model was 0.25 mL. This would explain why the approximate desorption temperature derived from the calculated adsorption energy lies in the lower region of the experimental desorption temperature range. Calculations at a lower surface coverage, using a $p(3 \times 3)$ unit cell, were also performed, giving an adsorption energy for methylamine of −0.83 eV, which corresponds to a desorption temperature of 332 K, in good agreement with the experimental results.

The adsorption geometry of methylamine on Ni(111) was quite similar to the corresponding gas-phase geometry [44], indicating no significant activation for this molecule when adsorbed on the Ni(111) surface. In fact, although both methylamine and ammonia are adsorbed through the nitrogen lone pair, the stronger adsorption of methylamine is what makes the dehydrogenation of CH_3NH_2 possible on the Ni(111) surface [21] (more difficult for a molecule that is not strongly adsorbed on the metal surface). We also calculated the adsorption energy of ammonia and confirmed this observation; the DFT adsorption energy of NH_3 was −0.41 eV, 0.15 eV lower than the corresponding one for methylamine. In another experimental study, the adsorption site of methylamine was characterized by RAIRS [29]: a C_s symmetry site in which the NH_2 group is held parallel to the surface plane and the CH_3 group is tilted away from the surface normal was described for this molecule. Our DFT calculations also gave this type of adsorption configuration for CH_3NH_2 on Ni(111) (Fig. 3).

3.4. HCN hydrogenation reaction mechanism

The hydrogenation reaction of nitriles has been reported to evolve go through an imine intermediate. In the hydrogenation reaction of hydrogen cyanide to methylamine, we also considered such an imine intermediate; methanimine. There are,

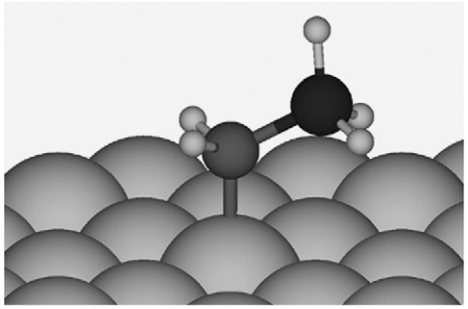

Fig. 3. Adsorption of H_3CNH_2 on Ni(111).

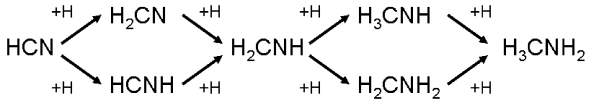

Scheme 1. Hydrogenation steps from HCN to H_3CNH_2.

however, two different reaction pathways that lead to methanimine; (1) hydrogenation of the carbon atom to yield H_2CN, followed by hydrogenation of the nitrogen atom to methanimine, and (2) hydrogenation of the nitrogen atom to yield HCNH, followed by hydrogenation of the carbon atom to form methanimine. From methanimine, the hydrogenation reaction can also follow two different routes: (1) hydrogenation of the carbon atom to yield H_3CNH, followed by hydrogenation of the nitrogen atom to form methylamine, and (2) hydrogenation of the nitrogen atom to form H_2CNH_2, followed by hydrogenation of the carbon atom giving methylamine (Scheme 1).

Fig. 4 shows the reaction energy profile of the hydrogenation reaction of HCN to CH_3NH_2. The reference energy used corresponds to the energy of the HCN + 4H system (energy of HCN adsorbed plus four times the energy of one adsorbed hydrogen atom). The energies of the $HCN_{(g)} + 2H_{2(g)}$ and $HCN_{(g)} + 4H$ systems are also indicated. For each elementary step, the coadsorption system formed by the reactant species and a hydrogen atom, shown in Fig. 4, has been used as starting point in the CI-NEB calculation. It can be seen how the adsorption energy of HCN was 1.13 eV with H present on the Ni(111) surface and 1.50 eV with no H present.

In first elementary step, the hydrogen atom can react with the nitrogen atom to yield HCNH or with the carbon atom to yield H_2CN. Both reactions are thermoneutral (i.e., the reaction energy is zero or almost zero), although the formation of HCNH is slightly more endothermic. The activation energy for the reaction of formation of HCNH is 1.39 eV (TS1). On the other hand, the activation energy for the $HCN + H \rightarrow H_2CN$ step is 1.13 eV (TS2). Therefore, it is easier to hydrogenate the carbon atom of HCN and to form H_2CN. As we will show later, this is, indeed, the rate-limiting step for the HCN hydrogenation reaction on Ni(111).

The activation energies for the reverse reactions, $H_2CN \rightarrow HCN + H$ and $HCNH \rightarrow HCN + H$, are 1.14 and 1.35 eV, respectively. Experimentally, small amounts of HCN were observed at temperatures around 540 K in a TPD study of methylamine dehydrogenation on Ni(111) [21]. Taking into account that the desorption temperature of HCN is between 180 and

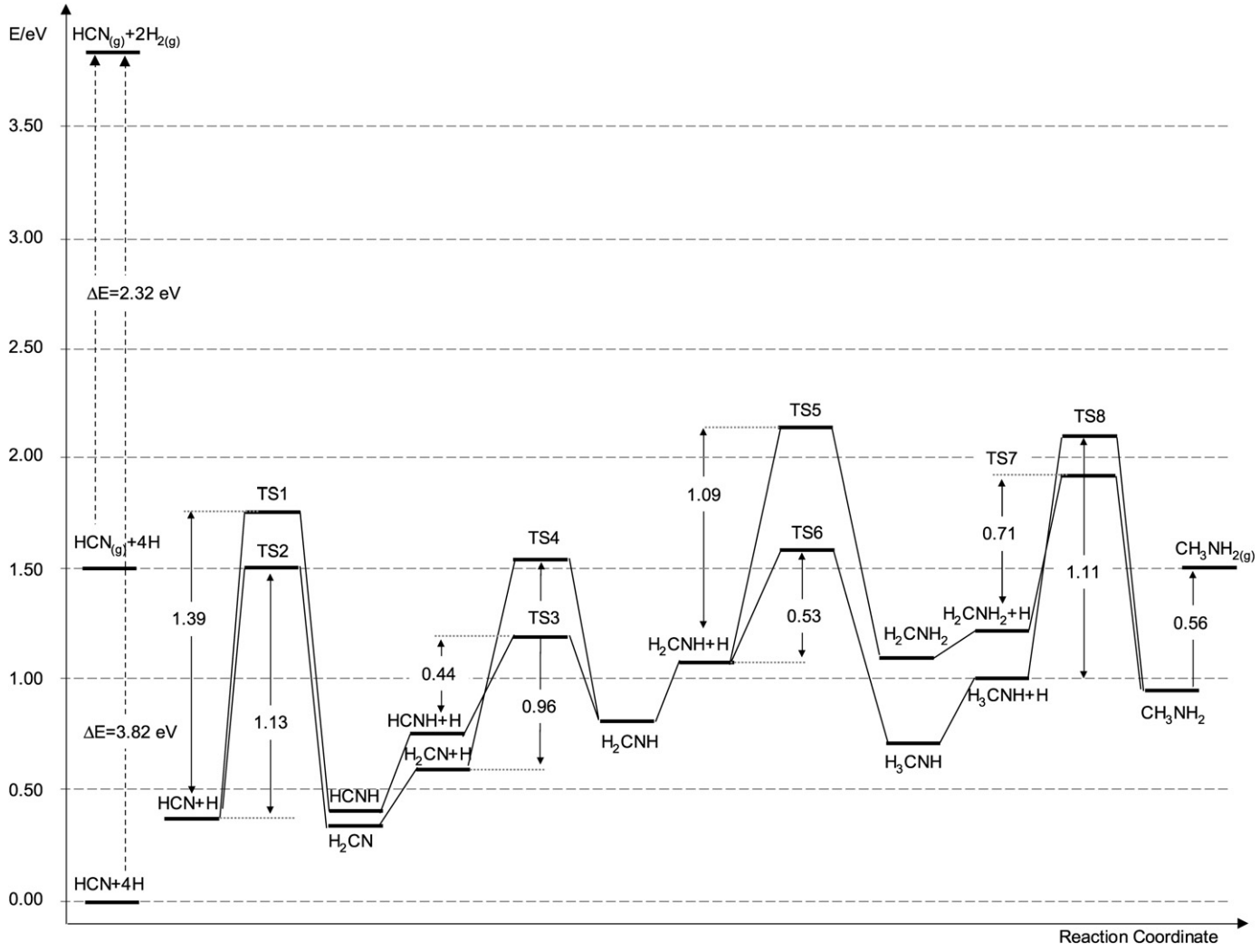

Fig. 4. Reaction energy profile for the hydrogenation of HCN to H_3CNH_2 on Ni(111).

Table 3
Geometric and energetic data of the intermediates involved in HCN hydrogenation on Ni(111)

Configuration		$E_{reaction}$[a] (eV)	d_{CN} (Å)	d_{NH} (Å)	d_{CH} (Å)	∠HCN (°)	∠HNC (°)	∠HCNH (°)	z-N[b] (Å)	z-C (Å)
H_2CN	f-η^3(N)	0.36	1.31	–	1.10	120	–	180	1.25	–
HCNH	h-η^2(C,N)	0.41	1.36	1.03	1.11	118	120	4	1.58	1.53
H_3CNH	b-η^2(N)	0.72	1.48	1.03	1.11	111	108	60	1.58	2.68
H_2CNH_2	f-η^1(N)-η^2(C)	1.10	1.48	1.03	1.12	111	112	122	2.00	1.67

[a] Calculated as the energy of the following reactions: $HCN_{(ads)} + 4H_{(ads)} \rightarrow H_2CN_{(ads)} + 3H_{(ads)}$, $HCN_{(ads)} + 4H_{(ads)} \rightarrow HCNH_{(ads)} + 3H_{(ads)}$, $HCN_{(ads)} + 4H_{(ads)} \rightarrow H_3CNH_{(ads)} + 1H_{(ads)}$, $HCN_{(ads)} + 4H_{(ads)} \rightarrow H_2CNH2_{(ads)} + 1H_{(ads)}$.

[b] z-X is the height of X to the Ni(111) surface.

330 K, the desorption of HCN at 540 K during the decomposition of methylamine, which corresponds to an energy requirement of approximately 1.35 eV, can be interpreted as the apparent activation energy for the dehydrogenation of either H_2CN or HCNH on Ni(111). This result agrees with the calculated activation energy for the dehydrogenation of HCNH step and is slightly larger than the activation energy for the $H_2CN \rightarrow HCN + H$ step. From our calculations, it is likely that the decomposition of methylamine to hydrogen cyanide occurs via the formation of the HCNH species, because, as we shall see later, it is more favorable to form HCNH from the methanimine intermediate instead of H_2CN. The formation of a HCNH intermediate during the decomposition of methylamine on Pt(111) also has been described [55].

For H_2CN, the most stable adsorption site corresponds to the f-η^3(N) site (Table 3) with the CN perpendicular to the nickel surface, whereas for HCNH, the preferred adsorption site is a h-η^2(C,N) site with the CN bond parallel to the surface. In the latter configuration, both carbon and nitrogen atoms interact with the metal surface and are located at around 1.50 Å

above the surface. The structures of TS1 and TS2 are shown in Fig. 5; in both cases, we can see how the C/N–H distance is being formed. The N–H and C–H distances are 1.50 Å and 1.35 Å for TS1 and TS2, respectively. In both transition state structures, the attacking H atom is at around 1.60 Å above the metal surface.

The second step in the reaction mechanism corresponds to the formation of methanimine, the imine intermediate. Methanimine can be formed either through hydrogenation of HCNH or H_2CN. Fig. 4 shows that the coadsorption of either HCNH or H_2CN with hydrogen, (HCNH + H) and (H_2CN + H), results in a destabilization of the system with respect to the H-free system. The second hydrogenation step is thermoneutral with respect to HCNH + H and slightly endothermic with respect to H_2CN + H. Our calculations show that it is easier to hydrogenate the carbon atom on HCNH than the nitrogen atom on H_2CN. The activation energy of the former elementary step is 0.44 eV (TS3), whereas that of the latter is 0.96 eV (TS4). Note that although the formation of HCNH is less favored than that of H_2CN in the first elementary step ($E_{TS1} > E_{TS2}$), it is significantly much easier to hydrogenate HCNH to H_2CNH than H_2CN ($E_{TS4} > E_{TS3}$). Therefore, it might be possible that H_2CN undergoes isomerization to form HCNH directly by hydrogen migration and then hydrogenation to H_2CNH.

Regarding the transition state geometries for these steps, the C···H distance is 1.61 Å in TS3, and the N···H distance is 1.48 Å in TS4. The distance of the attacking hydrogen atom to the surface is around 1.40 Å for both transition states (Fig. 6). Note how the CN bond in TS4 is tilted with respect to the surface normal; the CN is perpendicular in the case of the reactant and parallel in the case of the product. This could explain why the energy barrier for this step is higher than that corresponding to the TS3.

Once the imine intermediate is formed on the nickel surface, this can undergo subsequent hydrogenation to give H_3CNH or H_2CNH_2 (Scheme 1). As in the previous steps, the coadsorption of the imine intermediate with hydrogen results in a destabilization of methanimine. Our results show that the hydrogenation of methanimine on the carbon atom to give H_3CNH is easier (activation energy of 0.53 eV) (TS6) than the hydrogenation of the same intermediate on the nitrogen atom to give H_2CNH_2 (activation energy of 1.09 eV) (TS5). Furthermore, the elementary step leading to the formation of H_3CNH is exothermic with respect to H_2CNH + H, whereas the step that forms H_2CNH_2 is slightly endothermic; H_3CNH is actually 0.38 eV more stable than H_2CNH_2.

In terms of the structure of these intermediates, the H_3CNH fragment is adsorbed on a bridge site with the CN bond tilted away from the surface, and the N atom at 1.58 Å from it. The H_2CNH_2 species is adsorbed on an fcc hollow site (f-η^1(N)-η^2(C)), with both carbon and nitrogen atoms interacting with the surface metal atoms. In both species, the CN bond length is already quite close to that in methylamine (∼1.48 Å). In the structures of the transition states located for those reaction steps, TS5 and TS6, it can be seen how in both optimized structures the H_2CNH skeleton is quite similar (Fig. 7), with the only

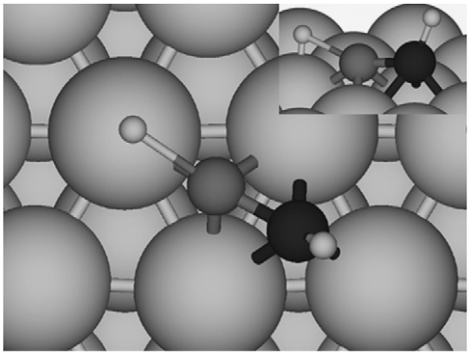

(a) TS1

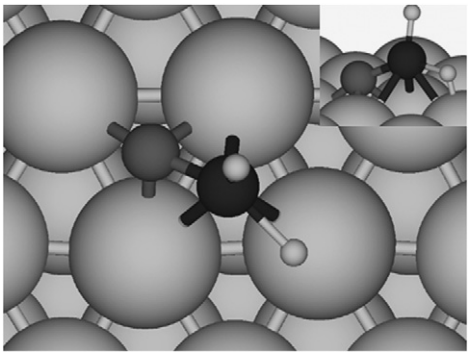

(b) TS2

Fig. 5. Transition states corresponding to the first hydrogenation step of HCN: (a) (TS1) HCN + H → HCNH and (b) (TS2) HCN + H → H_2CN.

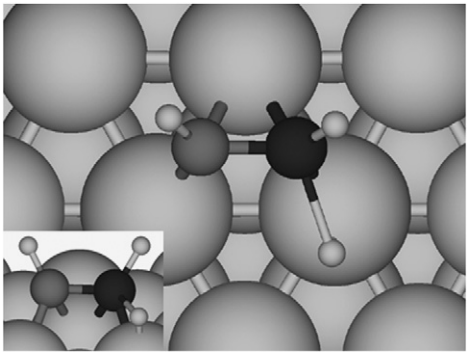

(a) TS3

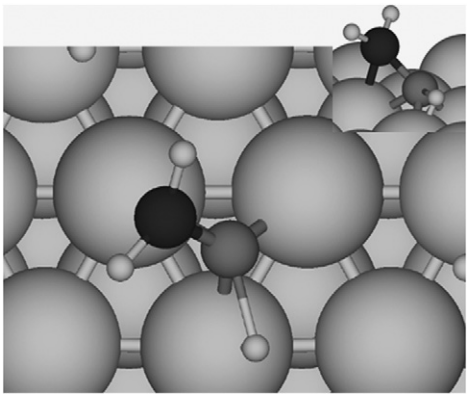

(b) TS4

Fig. 6. Transition states corresponding to the formation of the methanimine intermediate in the second hydrogenation step: (a) (TS3) HCNH + H → H_2CNH and (b) (TS4) H_2CN + H → H_2CNH.

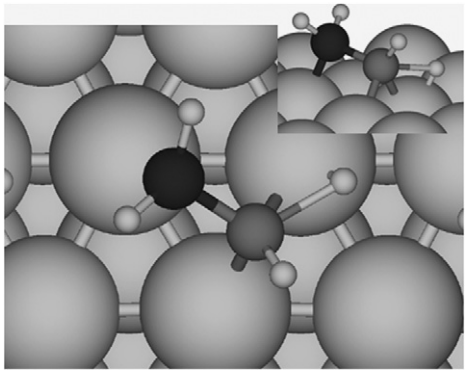

(a) TS5

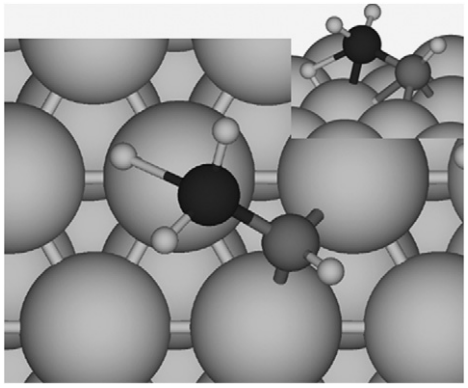

(b) TS6

Fig. 7. Transition states corresponding to the third hydrogenation step: (a) (TS5) $H_2CNH + H \rightarrow H_2CNH_2$ and (b) (TS6) $H_2CNH + H \rightarrow H_3CNH$.

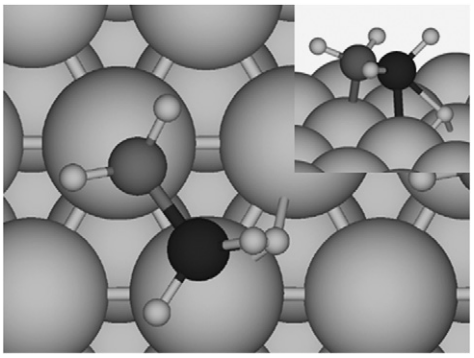

(a) TS7

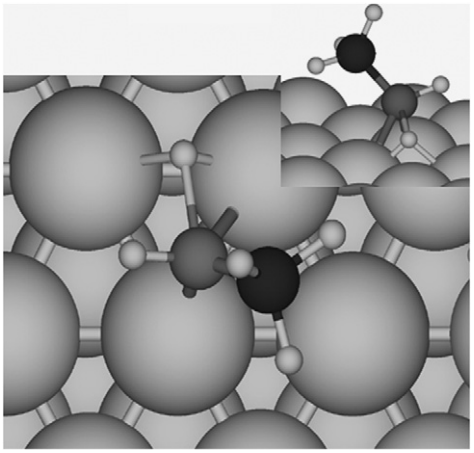

(b) TS8

Fig. 8. Transition states corresponding to the final hydrogenation step: (a) (TS7) $H_2CNH_2 + H \rightarrow H_3CNH_2$ and (b) (TS8) $H_3CNH + H \rightarrow H_3CNH_2$.

difference in the side (carbon or nitrogen) of approximation of the attacking hydrogen atom. This may indicate why the nitrogen atom is more difficult to hydrogenate than the carbon atom; because of the repulsive interaction between the attacking H atom and the N lone pair, in both cases, the H atom is at a similar distance from the atom to attack: ∼1.5 Å.

The final hydrogenation step corresponds to the formation of the primary amine. Fig. 4 shows that the coadsorption of either H_3CNH or H_2CNH_2 with hydrogen results in a destabilization with respect to the H-free system. The destabilization is larger for the $H_2CNH_2 + H$ system than for the $H_3CNH + H$ system. The greater destabilization of the system when the hydrogen atom is closer to the nitrogen atom can be rationalized in terms of a stronger repulsion interaction between the lone pair of the nitrogen atom and the hydrogen atom. This argument has also been used to explain the greater activation energies calculated for nitrogen hydrogenation than for carbon hydrogenation. Methylamine formation is thermoneutral with respect to $H_3CNH + H$ and slightly exothermic with respect to $H_2CNH_2 + H$. Although formation of the H_2CNH_2 intermediate is more difficult than formation of the H_3CNH intermediate ($E_{TS5} > E_{TS6}$), hydrogenation on the carbon atom ($H_2CNH_2 + H$, $E_{TS7} = 0.71$ eV) is again easier than hydrogenation on the nitrogen atom ($H_3CNH + H$, $E_{TS8} = 1.11$ eV). Therefore, it might be possible that H_3CNH undergoes isomerization to H_2CNH_2 and then reacts with hydrogen to yield methylamine. Concerning the transition states structures (TS7 and TS8), Fig. 8 shows that both the N···H and C···H distances are around 1.52 Å and that the H atom is at 1.1–1.2 Å above the nickel surface.

The final step in the hydrogenation reaction is the desorption of the product; methylamine. The calculated adsorption energy of methylamine at 0.25 mL is −0.56 eV, which would correspond to a desorption temperature of approximately 224 K. This value lies in the lower region of desorption temperatures reported experimentally (see the earlier discussion of methylamine). Furthermore, the total change in the calculated reaction energy for the hydrogenation of hydrogen cyanide to methylamine is −2.39 eV. This reaction energy is lowered to −1.67 eV taking into account the experimental zero-point energy correction [56]; which energy agrees with the experimental enthalpy of reaction at 298 K of −1.60 eV calculated from the enthalpies of formation of the reactants and products [57].

3.5. CH_3NH_2 dehydrogenation

The decomposition of methylamine has been studied experimentally on Ni(111) [21]. TPD experiments showed that the dehydrogenation of methylamine began at around 330 K, corresponding to an approximate energy requirement of 0.82 eV. In addition, the H_2 TPD spectrum showed a desorption peak between 363 (∼0.91 eV) and 390 K (∼0.98 eV). This means that the energy needed to remove the first hydrogen from methylamine ranged between 0.82 and 0.98 eV. In addition, isotopic

labeling experiments with deuterium showed that in the case of Ni(111), the C–H bond broke more easily than the N–H bond, the opposite of that was observed on Pd(111) [26] or Pt(111) [55]. Our DFT calculations indeed show that hydrogen atoms of the methyl group were more labile than those of the amine group, and thus it is easier to break the C–H bond than the N–H bond on Ni(111). The calculated activation energy for breaking the first C–H bond yielding to $H_2CNH_2 + H$ is 0.99 eV (Fig. 4, TS7, reverse reaction). This activation energy is in agreement with the experimental TPD data. On the other hand, the activation energy for breaking the N–H bond is 1.17 eV, again confirming the experimental findings. The activation energy for the C–N bond cleavage of methylamine on Ni(111) has been studied theoretically [32]; a value of 1.49 eV was reported, clearly greater than the activation energy calculated in this work for either C–H or N–H bond breaking. In fact, it has been described experimentally that methylamine decomposition is likely to occur by C–N bond cleavage on Ni(100) [31] and by C–H bond-cleavage on Ni(111).

4. Conclusions

From our study of the adsorption and hydrogenation of hydrogen cyanide to methylamine on Ni(111), several conclusions can be inferred:

1. Hydrogen cyanide adsorbs with the CN bond parallel to the surface with an adsorption energy of −1.50 eV at 0.25 mL (using the PW91 exchange-correlation functional). This adsorption energy is overestimated if we compare with the available experimental data. Better agreement with the experimental data can be achieved using the RPBE exchange-correlation functional; in this case, the adsorption energy of HCN is −0.90 eV.
2. The rate-limiting step is the first hydrogenation step. Two different pathways are possible: (1) hydrogenation of the carbon atom, yielding H_2CN, and (2) hydrogenation of the nitrogen atom, yielding HCNH. The activation energy is 1.13 eV for H_2CN formation and 1.35 eV for HCNH formation. Further, H_2CN is slightly more stable than HCNH, and, consequently, the formation of H_2CN is favored with respect to HCNH.
3. The hydrogenation reaction proceeds via an imine intermediate, H_2CNH, which can be formed by hydrogenating either the nitrogen atom of the H_2CN species or the carbon atom of the HCNH species. Thus, it may be concluded that HCN is hydrogenated first to H_2CN and then to H_2CNH. However, it is also possible that H_2CN undergoes isomerization to HCNH, followed by hydrogenation to H_2CNH.
4. Methanimine is hydrogenated preferentially to H_3CNH rather than to H_2CNH_2. The attack of the hydrogen atom to the nitrogen atom is hindered by the extra repulsion term between the electron density of the reactive hydrogen atom and the lone pair of the nitrogen atom (TS6).
5. Methylamine is formed by hydrogenation of either H_2CNH_2 or H_3CNH. The activation energy is lower starting from H_2CNH_2, but H_3CNH is preferentially formed from H_2CNH. Therefore, we can conclude that methylamine is formed by hydrogenation of H_3CNH. However, as in point 3, it is also possible that H_3CNH species first undergoes isomerization to H_2CNH_2, followed by hydrogenation of H_2CNH_2 to methylamine.
6. The calculated adsorption energy of methylamine is −0.56 eV at 0.25 mL and −0.82 eV at 0.11 mL. From these results, we can conclude that methylamine desorbs from the Ni(111) surface at 224–332 K, which is in good agreement with experimental results. Compared with ammonia, methylamine adsorbs more strongly on Ni(111), which may explain why it undergoes decomposition on Ni(111) whereas ammonia does not.
7. In the case of the reverse reaction, the decomposition of methylamine on Ni(111), our calculations show that it is easier to first break the C–H bond than the N–H bond. This result agrees with isotopic labeling experiments with deuterium demonstrating that the hydrogen atoms of the methyl group are more labile than those of the amine group. The activation energy for the cleavage of the first C–H bond is 0.99 eV.

Acknowledgments

The authors thank the Stichting Nationale Computerfaciliteiten (NCF) for providing supercomputer time at SARA in Amsterdam. C.O. acknowledges the European Union for a Marie-Curie Fellowship. D.C. acknowledges support through NWO VENI Grant 700-53-403.

References

[1] J. Volf, J. Pasek, in: L. Cerveny (Ed.), Studies in Surface Science and Catalysis, vol. 27, Elsevier, Amsterdam, 1986, p. 105.
[2] L. Hegedűs, T. Máthé, Appl. Catal. A 296 (2005) 209.
[3] P. Kukula, M. Studer, H.U. Blaser, Adv. Synth. Catal. 346 (2004) 1487.
[4] P. Kukula, K. Kopriovova, J. Catal. 234 (2005) 161.
[5] M.J.F.M. Verhaak, A.J. van Dillen, J.W. Geus, J. Catal. 143 (1993) 187.
[6] C.V. Rode, M. Arai, M. Shirai, Y. Nishiyama, Appl. Catal. A 148 (1997) 405.
[7] B. Bigot, F. Delbecq, A. Milet, V.H. Peuch, J. Catal. 159 (1996) 383.
[8] M.E. Kordesch, Th. Lindner, J. Somers, W. Stenzel, H. Conrad, A.M. Bradshaw, G.P. Williams, Spectrochim. Acta A 43 (1987) 1561.
[9] J.G. Serafin, C.M. Friend, J. Phys. Chem. 92 (1988) 6694.
[10] H. Celio, P. Mills, D. Jentz, Y.I. Pae, M. Trenary, Langmuir 14 (1998) 1379.
[11] H. Celio, P. Mills, D. Jentz, M. Trenary, Surf. Sci. 381 (1997) 65.
[12] R.M. Van Hardeveld, A.J.G.W. Schmidt, R.A. van Santen, J.W. Niemantsverdriet, J. Vac. Sci. Technol. A 15 (1997) 1642.
[13] R.M. Van Hardeveld, R.A. van Santen, J.W. Niemantsverdriet, J. Phys. Chem. B 101 (1997) 7901.
[14] P.L. Hagans, I. Chorkendorff, J.T. Yates Jr., J. Phys. Chem. 92 (1988) 471.
[15] K.L. Shanahan, E.L. Muetterties, J. Phys. Chem. 88 (1984) 1996.
[16] K.A. Pearlstine, C.M. Friend, J. Phys. Chem. 90 (1986) 4341.
[17] X. Guo, A. Hoffman, J.T. Yates Jr., J. Phys. Chem. 93 (1989) 4253.
[18] K. Murphy, S. Azad, D.W. Bennett, W.T. Tysoe, Surf. Sci. 467 (2000) 1.
[19] H.Y. Yang, J.L. Whitten, J. Phys. Chem. 100 (1996) 5090.
[20] J.M. Hu, Y. Li, J.-Q. Li, Y.-F. Zhang, L.-X. Zhou, Act. Chim. Sin. 61 (2003) 476.
[21] I. Chorkendorff, J.N. Russell Jr., J.T. Yates Jr., J. Chem. Phys. 86 (1987) 4692.
[22] G.R. Schoofs, J.B. Benziger, J. Phys. Chem. 92 (1988) 741.
[23] C. Chang, C. Khong, R. Saiki, J. Vac. Sci. Technol. A 11 (1993) 2122.

[24] M.E. Bridge, J. Somers, Vacuum 38 (1988) 317.
[25] D. Jentz, M. Trenary, X.D. Peng, P. Stair, Surf. Sci. 341 (1995) 282.
[26] J.J. Chen, N. Winograd, Surf. Sci. 326 (1995) 285.
[27] K.A. Pearlstine, C.M. Friend, J. Am. Chem. Soc. 108 (1986) 5842.
[28] R.W. Sheets, G. Blyholder, J. Catal. 67 (1981) 308.
[29] T.S. Nunney, J.J. Birtill, R. Raval, Surf. Sci. 427–428 (1999) 282.
[30] S.Y. Hwang, A.C.F. Kong, L.D. Schmidt, J. Phys. Chem. 93 (1989) 8327.
[31] A.G. Baca, M.A. Schulz, D.A. Shirley, J. Chem. Phys. 83 (1985) 6001.
[32] J. Li, R.-F. Li, G.-C. Wang, J. Phys. Chem. B 110 (2006) 14300.
[33] G. Kresse, J. Hafner, Phys. Rev. B 47 (1993) 558.
[34] G. Kresse, J. Furthmüller, Phys. Rev. B 54 (1996) 11169.
[35] J.P. Perdew, J.A. Chevary, S.H. Vosko, K.A. Jackson, M.R. Pederson, D.J. Singh, C. Fiolhais, Phys. Rev. B 46 (1992) 6671.
[36] Y. Wang, J.P. Perdew, Phys. Rev. B 44 (1991) 13298.
[37] P.E. Blöchl, Phys. Rev. B 50 (1994) 17953.
[38] G. Kresse, J. Joubert, Phys. Rev. B 59 (1999) 1758.
[39] M. Methfessel, A.T. Paxton, Phys. Rev. B 40 (1989) 3616.
[40] H.J. Monkhorst, J.D. Pack, Phys. Rev. B 13 (1972) 5188.
[41] C. Kittel, in: Introduction to Solid State Physics, seventh ed., Wiley, New York, 1996.
[42] P. Pulay, Chem. Phys. Lett. 73 (1980) 393.
[43] G. Henkelmann, B.P. Uberuaga, H. Jónsson, J. Chem. Phys. 113 (2000) 9901.
[44] G. Herzberg, Electronic Spectra and Electronic Structure of Polyatomic Molecules, Van Nostrand, New York, 1966.
[45] C.-M. Chan, R. Aris, W.H. Weinberg, Appl. Surf. Sci. 1 (1978) 360.
[46] G. Kresse, A. Gil, P. Sautet, Phys. Rev. B 68 (2003) 073401.
[47] M. Gajdos, A. Eichler, J. Hafner, J. Phys. Condens. Matter 16 (2004) 1141.
[48] M. Gajdos, J. Hafner, A. Eichler, J. Phys. Condens. Matter 18 (2006) 13.
[49] S.E. Mason, I. Grinberg, A.M. Rappe, Phys. Rev. B 69 (2004) 161401.
[50] J.P. Perdew, K. Burke, M. Ernzerhof, Phys. Rev. Lett. 77 (1996) 3865.
[51] Y. Zhang, W. Yang, Phys. Rev. Lett. 80 (1998) 890.
[52] B. Hammer, L.B. Hansen, J.K. Norskov, Phys. Rev. B 59 (1999) 7413.
[53] Z. Knor, Surf. Sci. 154 (1985) L233.
[54] M.D. Harmony, V.W. Laurie, R.L. Kuczkowski, R.H. Schwendeman, D.A. Ramsay, F.J. Lovas, W.J. Lafferty, A.G. Maki, J. Phys. Chem. Ref. Data 8 (1979) 619.
[55] W. Erley, J.C. Hemminger, Surf. Sci. 316 (1994) L1025.
[56] T. Shimanouchi, Tables of Molecular Vibrational Frequencies (NSRDS-NBS), consolidated vol. 1, National Bureau of Standards, 1972, http://webbook.nist.gov/chemistry.
[57] M. Frenkel, K.N. Marsh, R.C. Wilhoit, G.J. Kabo, G.N. Roganov, Thermodynamics of Organic Compounds in the Gas State, Thermodynamics Research Center, College Station, TX, 1994, http://webbook.nist.gov/chemistry.